ENVIRONMENTAL ENGINEERING SCIENCE
Volume 30, Number 4, 2013

DOI: 10.1089/ees.2012.0337

Dissolution-Driven Permeability Reduction of a Fractured Carbonate Caprock

Brian R. Ellis,[1] Jeffrey P. Fitts,[1] Grant S. Bromhal,[2] Dustin L. McIntyre,[2] Ryan Tappero,[3] and Catherine A. Peters[1,*]

[1]*Department of Civil and Environmental Engineering, Princeton University, Princeton, New Jersey.*
[2]*National Energy Technology Laboratory, U.S. Department of Energy, Morgantown, West Virginia.*
[3]*Photon Sciences Department, Brookhaven National Laboratory, U.S. Department of Energy, Upton, New York.*

Received: August 24, 2012 *Accepted in revised form: January 8, 2013*

Abstract

Geochemical reactions may alter the permeability of leakage pathways in caprocks, which serve a critical role in confining CO_2 in geologic carbon sequestration. A caprock specimen from a carbonate formation in the Michigan sedimentary Basin was fractured and studied in a high-pressure core flow experiment. Inflowing brine was saturated with CO_2 at 40°C and 10 MPa, resulting in an initial pH of 4.6, and had a calcite saturation index of −0.8. Fracture permeability decreased during the experiment, but subsequent analyses did not reveal calcite precipitation. Instead, experimental observations indicate that calcite dissolution along the fracture pathway led to mobilization of less soluble mineral particles that clogged the flow path. Analyses of core sections via electron microscopy, synchrotron-based X-ray diffraction imaging, and the first application of microbeam Ca K-edge X-ray absorption near edge structure, provided evidence that these occlusions were fragments from the host rock rather than secondary precipitates. X-ray computed tomography showed a significant loss of rock mass within preferential flow paths, suggesting that dissolution also removed critical asperities and caused mechanical closure of the fracture. The decrease in fracture permeability despite a net removal of material along the fracture pathway demonstrates a nonintuitive, inverse relationship between dissolution and permeability evolution in a fractured carbonate caprock.

Key words: calcite dissolution, caprock integrity; CO_2 sequestration; fracture flow, fines migration; leakage

Introduction

The success of geologic carbon sequestration in deep saline formations will rely heavily on our ability to estimate the leakage risks associated with underground storage of large quantities of a buoyant fluid. The existence of potential CO_2 leakage pathways and estimates of CO_2 leakage have been discussed extensively in the literature (Lewicki *et al.*, 2007; Celia and Nordbotten, 2009; Shukla *et al.*, 2010). However, current leakage risk assessment models (*e.g.*, LeNeveu, 2008; Viswanathan *et al.*, 2008) do not account for geochemical alterations of potential leakage pathways in caprock formations, and thus, may estimate inaccurate CO_2 or brine leakage rates along a reactive pathway, such as that of a fractured carbonate caprock (Ellis *et al.*, 2011).

Geochemical reactions that alter caprock integrity may occur over short time periods, as demonstrated in bench-scale experimental investigations (Kaszuba *et al.*, 2005; Andreani *et al.*, 2008; Wigand *et al.*, 2009; Shao *et al.*, 2010; Ellis *et al.*, 2011; Smith *et al.*, 2013). In particular, CO_2 injection into deep saline aquifers will cause acidification of formation brines (Ellis *et al.*, 2010) and carbonate minerals are susceptible to acid-driven dissolution (Pokrovsky *et al.*, 2009). Therefore, understanding the potential alterations of carbonate caprocks due to reaction with CO_2-acidified brine is a necessary first step toward predicting leakage through these formations. In the context of geologic carbon sequestration, Gherardi *et al.* (2007) simulated enhanced sealing at the caprock-reservoir interface when carbonate precipitation occurs where mass transport of reactive fluids is limited by slow diffusion into the caprock. Similar self-sealing behavior has been observed in wellbore cements (Huerta *et al.*, 2011). Conditions that favor carbonate mineral precipitation within advection-controlled leakage pathways may require mixing of higher-pH interstitial waters with calcium- and carbonate-enriched reservoir brines (Zhang *et al.*, 2010; Nogues *et al.*, 2012). Core flow studies conducted at ambient conditions and low CO_2 partial pressure have demonstrated complex alterations along limestone fracture pathways (Gouze *et al.*, 2003; Noiriel *et al.*, 2007).

This work contributes to the current knowledge, by examining the potential for mineral dissolution and precipitation to alter the permeability of fractured carbonate caprocks

**Corresponding author:* Department of Civil and Environmental Engineering, Princeton University, Princeton, NJ 08540. *Phone:* (609) 258-5645; *Fax:* (609) 258-2799; *E-mail:* cap@princeton.edu

Table 1. Imaging Methods and Their Applications in This Study

Imaging method	*Analysis*	*Purpose in this study*
Scanning electron microscopy and energy dispersive X-ray spectroscopy	2D thin sections of core cross-sections	To map Ca and Mg distribution at the fracture boundary and of occlusions within the fracture with surface sensitivity.
Micro X-ray computed tomography	3D scans of the entire core	To quantify rock mass removal from the fracture surface, determine where there was the greatest occlusion of flow, and examine the evolution of fracture roughness.
X-ray fluorescence	2D thin sections of core cross-sections	To map Ca composition.
X-ray diffraction	2D thin sections of core cross-sections	To identify crystalline phases of fracture occlusions.
X-ray adsorption near edge structure	2D thin sections of core cross-sections	To determine Ca-speciation and identify the origin of the occlusions.

under reservoir temperature and pressure conditions relevant to carbon sequestration. This article presents results from a high-pressure core flow experiment in which CO_2-acidified brine flowed through an artificially-fractured carbonate caprock sample. The core sample used in this study is from the Amherstburg limestone, which serves as the primary caprock for a CO_2 injection demonstration project into the Bass Islands formation in northern Michigan. This experiment builds upon our previous study (Ellis *et al.*, 2011), since both experiments involved a rock specimen from the same formation and were conducted under reservoir temperature and pressure conditions. Both experiments were designed to examine how brine chemistry and mineral heterogeneity determine whether fractures will be widened or may self-seal when exposed to CO_2-saturated brine. The experiments were comparable with regard to pH, but in this experiment the calcite saturation in the brine was more than an order of magnitude closer to equilibrium (calcite saturation index $= -0.8$). This design allowed for the possibility that calcite saturation might occur within the fracture; thus, testing a hypothesis about precipitation-induced caprock sealing in the context of geologic carbon sequestration.

Because of the inherent difficulty in sampling CO_2-saturated fluids at high pressures, we did not rely solely on inferences from effluent solute concentrations. Instead, we relied on pressure gradient measurements and on a suite of imaging techniques to relate permeability evolution to changes in fracture morphology resulting from mineralogy-specific erosion and deposition processes (Table 1). Three-dimensional micro X-ray computed tomography (μCT) of the core was used to measure net changes in rock mass and morphological alterations of the fracture surface. After the experiment, the fracture was epoxy-stabilized and sectioned, and examined using a combination of electron microscopy and synchrotron-based X-ray spectroscopic and diffraction imaging. This included the development of new procedures for microbeam Ca K-edge X-ray absorption near edge structure (XANES) spectroscopy at the National Synchrotron Light Source (NSLS).

Small-scale, short-term experiments may not necessarily represent field-scale, long-term behavior of subsurface systems. However, controlled laboratory experiments such as this one provide a unique opportunity to gain insight into the complex physical and chemical processes affecting flow in a reactive rock. While this single core flow experiment cannot be interpreted in a statistical sense, the observations are valuable in revealing processes and phenomena that are possible. The aim of this study was to understand processes operative in a reactive carbonate rock exposed to CO_2-saturated brine, and then to re-examine existing paradigms about the performance of these rocks as caprock seals.

Materials and Methods

Sample characterization

The Amherstburg is a fossiliferous carbonate formation composed primarily of calcite and dolomite, in roughly equal proportions. Together, these minerals make up >90% of the bulk sample, with the remaining rock containing quartz, K-feldspar, clay minerals, and pyrite. For details on the mineral identification procedure, see Ellis *et al.* (2011). A subcore, 2.54 cm in diameter and 3.8 cm in length, was taken from a drilling core sampled at 928 m, oriented vertically. A flow path was created by fracturing the dry core using dual knife-edge chisels. Before and after fracturing, the core exterior was stabilized in epoxy (which was then machined to a uniform epoxy thickness) in order to ensure no displacement between the two core halves during handling.

Geochemical modeling of initial brine composition

The experimental brine was designed to represent a CO_2-saturated brine that had already reacted with minerals in the target injection formation, the Bass Islands formation dolostone. A batch of the synthetic brine was prepared by mixing deionized water and salts: NaCl (extra pure; Acros Organics), $CaCl_2$ (>96% pure; Acros Organics), $MgCl_2 \cdot 4H_2O$ (reagent grade ACS; Acros Organics), NaOH (>97% pure; Acros Organics), and Na_2SO_4 (>99% pure; Fisher), which was then contacted with pressurized CO_2. Specifically, the initial brine composition, shown in Table 2, mimicked a CO_2-saturated

Table 2. Inflowing Brine Composition

Species (total)	*[mol/L]*
Na^+	1.0×10^{0}
Cl^-	1.0×10^{0}
Ca^{2+}	2.9×10^{-2}
Mg^{2+}	2.6×10^{-3}
SO_4^{2-}	1.2×10^{-2}
$CO_{2(aq)}$	9.8×10^{-1}
pH	4.6

1 M NaCl brine reacted with anhydrite, calcite, and dolomite to an initial calcite saturation index of −0.8. PHREEQC was used to estimate initial mineral saturation indices and brine pH using the Pitzer.dat thermodynamic database (Pitzer, 1973; Parkhusrt and Appelo, 1999). CO_2 solubility was estimated to be 0.98 mol/L following the work of Duan *et al.* (2006). Activity coefficients of aqueous species were estimated using the Pitzer model (Pitzer, 1973). Brine pH was estimated to be 4.6 at equilibrium with 10 MPa CO_2 pressure.

Flow-through experiment

A similar flow-through setup as described in Ellis *et al.* (2011) was used to inject CO_2-saturated brine through the fractured core. A TEMCO triaxial carbon-fiber core holder was used with a confining pressure of 14 MPa. Two separate high-pressure syringe pumps (Teledyne Isco, Inc.) delivered CO_2 (99.5% pure; Airgas) and brine to a high-pressure mixing vessel where they equilibrated at 40°C. The measured pH was within ±0.2 of the modeled pH, verifying equilibrium. The pore pressure at core outlet of 10 MPa was maintained via back-pressure regulator. Measured inlet brine composition is shown in Table 2. Inlet pH was measured at system temperature and pressure with high-pressure pH probes (Corr Instruments, LLC). The pH probes at the flow outlet malfunctioned, thereby preventing measurement of brine effluent pH and subsequent estimation of effluent mineral saturation indices. Brine samples were stabilized with nitric acid and diluted before being analyzed via inductively coupled plasma optical emission spectrometry on a Perkin Elmer Optima 3000 XL.

The experiment was designed to have a constant flow rate of 3 mL/h. This constant flow rate was held only for the first 28 h of the experiment. After this, the flow was controlled by a constant pressure difference of ∼2.2 MPa due to a predetermined upper limit of 12.2 MPa for the inlet pore pressure. A temperature of 40°C was successfully maintained in the mixing vessel. Limitations in the maximum allowable surface temperature able to be applied to the carbon-fiber core holder prevented sufficient heating of the core holder to maintain the desired internal temperature of 40°C. The average temperature measured inside the core was 30°C and is therefore, the temperature used to estimate brine viscosity.

Estimation of fracture permeability

Fracture permeability, k, is calculated by first relating the measured pressure difference, ΔP, to an equivalent hydraulic aperture, b_h according to the cubic law for flow between two parallel plates (Zimmerman and Bodvarsson, 1996),

$$b_h = \sqrt[3]{\frac{12\mu LQ}{\Delta P w}} \tag{1}$$

where Q is the volumetric flow rate, μ is the viscosity of the fluid, L is the length of the fracture, and w is the fracture width. Although this equation assumes that the fracture walls are both parallel and smooth, which is often not the case for natural fractures, it is useful here in providing a first approximation of fracture hydraulic aperture. A brine viscosity of 0.90 mPa/s was calculated following Phillips *et al.* (1981). Fracture permeability was then estimated by combining the cubic law with Darcy's Law:

$$k = \frac{b_h^2}{12} \tag{2}$$

X-ray computed tomography

Using a MicroXCT-400 (μCT) scanner (Xradia, Inc.) to distinguish mineral and void space (Ketcham and Carlson, 2001), the fractured core was imaged before and after the experiment, dry and under ambient pressure. The X-ray beam energy was 150 keV and power was 10 W, with scan rotational increments of 0.14°. The 3D reconstructed image had a voxel resolution of 27 μm. The scans yielded good data for 2.4 cm of the total fracture width.

Electron microscopy and spectroscopic imaging

After the experiment and μCT scan, the core fracture was impregnated with epoxy using methods described by Crandell *et al.* (2012). The core was then sectioned perpendicular to the direction of flow. The samples were examined using a Quanta environmental scanning electron microscope (SEM) at a beam energy of 15 keV. The SEM was used for backscattered electron (BSE) imaging and energy dispersive spectroscopy (EDS).

At the NSLS (Brookhaven National Lab), X-ray microprobes at beamlines X27A and X26A were used. X-ray fluorescence maps were collected by raster "fly-scanning" the ∼7×10 (V×H) micron beam at 17.5 keV over regions of interest. Microbeam Ca K-edge XANES spectra were collected at points of interest. Beam energy was controlled with a ^{111}Si monochromator. Background subtraction, normalization, and linear combination fits (LCFs) were performed using Athena software (Ravel and Newville, 2005). X-ray diffraction point spectra were collected at 17.479(2) keV incident beam energy using either a Bruker or Rayonix CCD. The diffraction images were background subtracted and integrated into 1D intensity versus 2-theta using FIT2D (Hammersley *et al.*, 1996).

Results

Evolution of fracture permeability

The experiment lasted 3 days, and based on observed pressure changes, fracture permeability decreased over this time. There were two distinct periods: the first 28 h when the flow rate was held constant and the final 51 h when a constant pressure gradient was maintained. A linear regression of the pressure data for the first 28 h indicates a rate of change in ΔP of 0.074 MPa/h. During the final 51 h the flow rate was instead used to estimate permeability evolution. The time-averaged flow rate during this period was 0.6 mL/h, representing an approximate 80% reduction in flow rate. The observed ΔP is shown in Fig. 1 along with the corresponding evolution of fracture permeability. Over the course of the entire experiment, fracture permeability decreased more than an order of magnitude.

Effluent chemistry

Analysis of the Ca concentration in the collected brine effluent is given in Fig. 2. Figure 2 shows an initial increase in Ca

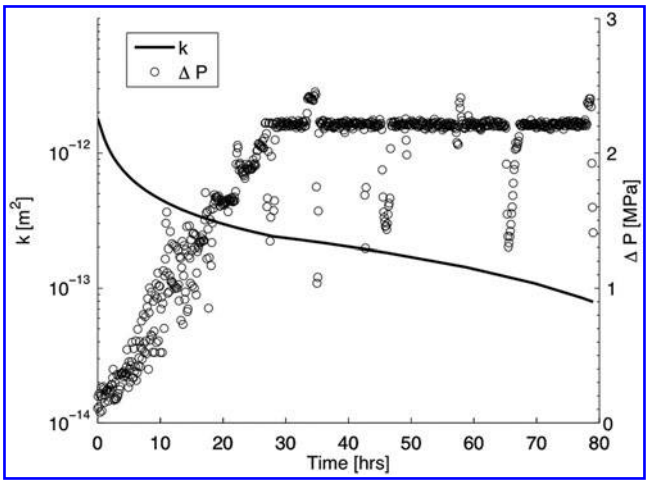

FIG. 1. Change in measured pressure difference across the core and corresponding best fit of permeability evolution. As the experimental flow conditions were switched from constant flow rate to constant pressure gradient at 28 h, two separate linear fits were used to describe permeability evolution over these two distinct flow regimes.

concentration followed by a decrease after cessation of the constant flow rate. The slowed flow rate may have created localized conditions of diffusion-controlled mass transport, and longer fluid residence times that resulted in calcite saturation. While this is an interesting finding, as is discussed later, spectroscopic imaging revealed little evidence of calcite precipitation.

X-ray μCT imaging

The μCT images were processed as described previously (Ellis *et al.*, 2011). The μCT data were used in this study to: (1) quantify and map rock mass removal from the fracture surface, (2) determine the regions of the fracture where there was the greatest occlusion of flow, and (3) examine the evolution of fracture roughness. Mechanical aperture data derived from the μCT scans do not represent the absolute magnitude of fracture apertures during the flow experiment because of compression under confining pressure. However, the relaxed core measurements do record net changes in mass removal along the fracture. The reproducibility of distances between distinct features in the scans of the two core halves confirmed that the halves returned to their original positions after depressurization. Therefore, the difference in void volume of the before and after scans is a measure of the change in rock mass along the fracture pathway.

Figure 3a and b portrays the fracture aperture maps. The increase in aperture variance provides information about the evolution of fracture roughness, which is consistent with previous findings (Ellis *et al.*, 2011),* and is explained by preferential dissolution of calcite.

The net changes in rock mass along the flow direction are shown in Fig. 3c. Summing the aperture changes over the entire fracture, it was determined that, in total, 50 mg of rock was dissolved. There was greater dissolution at the inlet of the core. There were regions near the outlet where there was a net increase in rock mass within the fracture. Figure 3b clearly depicts that this occurred in a region on the right side of the fracture. As is discussed below, in this region evidence of rock fragments within the fracture appears in the μCT scans as voxels with X-ray attenuation values similar to that of the rock matrix (see Fig. 4b). On the left side, a net increase in fracture aperture is observed, implying that a preferential flow path emerged there.

The principles of critical path analysis in percolation theory dictate that the most resistive paths will control the flow rate along a leakage pathway (Berkowitz and Balberg, 1993). Because we know that the fracture surfaces were not exactly parallel, it is possible that after confining stress was applied, the mechanical aperture near the outlet was restricting flow, while larger apertures emerged upstream.

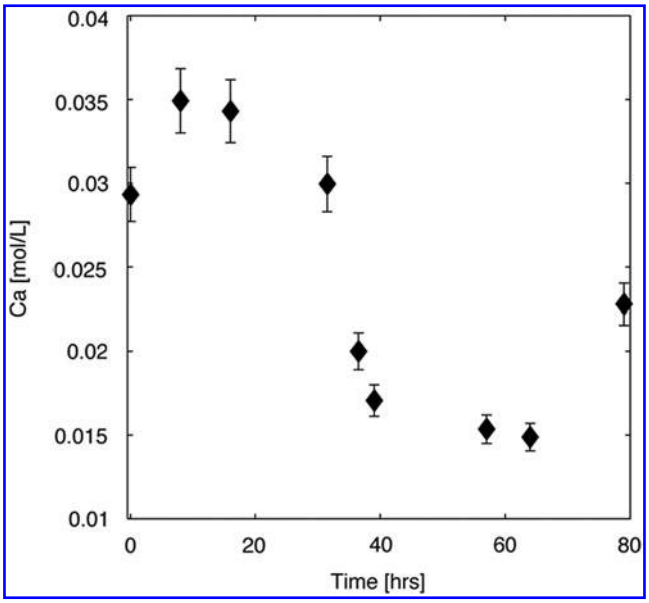

FIG. 2. Measured Ca concentration in brine effluent. Initial concentration (see Table 2) is shown at time = 0. The error bars represent the 95% confidence interval of the standard analytical error of 2.8% calculated from duplicate analyses of several brine effluent samples.

Electron microscopy and X-ray spectroscopic and diffraction imaging

Because the μCT analysis revealed regions of increased rock mass near the outlet of the core, a section was taken from that part of the core for subsequent 2D imaging analysis. Results are presented in Fig. 4 with the approximate location noted in Fig. 4a. Figure 4c and d reveals mineral fragments in the fracture. Because these fragments do not morphologically match the nearby fracture walls, it appears that they did not simply detach from the local surface but rather they have been transported from elsewhere in the flow path. It is likely that these fragments account for the added rock mass observed from the μCT data (see Fig. 3c).

Ca μXANES, EDS, and μXRD were used to identify the mineralogy of the fragments along the fracture pathway. The Ca μXANES spectra for the subset of points labeled A–D are shown in Fig. 4e along with the end-member spectra of

*Deng, H., Ellis, B.R., Peters, C.A., Fitts, J.P., Crandall, D., and Bromhal, G.S. (Unpublished study). Modifications of carbonate fracture hydrodynamic properties by CO_2-acidified brine flow. Princeton University, Princeton, NJ, 2012.

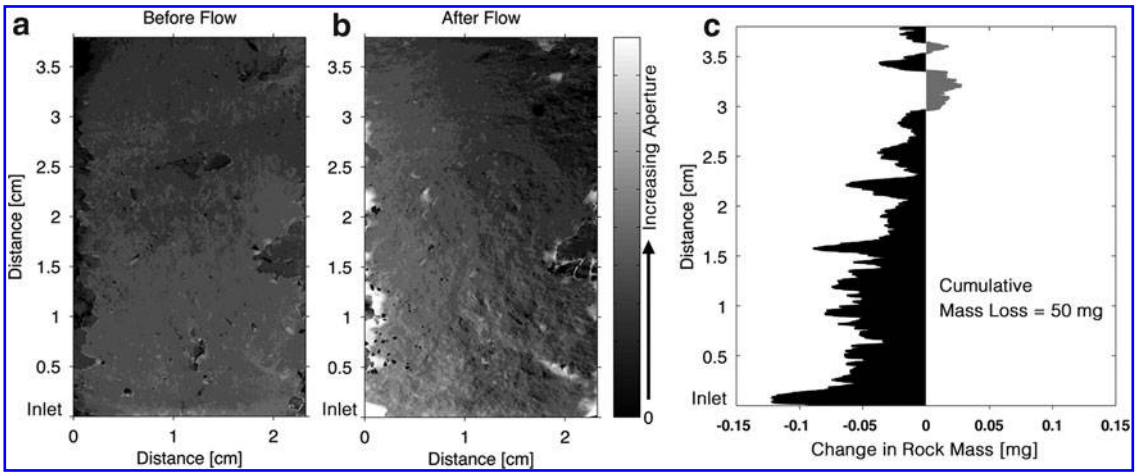

FIG. 3. Aperture maps, as estimated from the micro X-ray computed tomography (μCT) data, for the fracture before **(a)** and after **(b)** flow of the CO_2-acidified brine. The increased aperture variability shown in **(b)** is demonstrative of the increase in fracture roughness after flow. **(c)** The change in rock mass along the length of the fracture.

calcite and dolomite. LCF was used to estimate the relative composition of dolomite and calcite at each point. The smaller fragments (sites B and C) have a signal more similar to calcite, while there is a stronger contribution of dolomite in the larger fragments (site A). The fact that the larger fragments contain dolomite confirms that these particles must have been released from the upstream flow path, as dolomite precipitation is unlikely under the conditions of this experiment. Even though the other spectroscopic techniques (EDS, μXRD) did not confirm it, the Ca μXANES LCF shows the presence of dolomite also in the smaller fragments, so they are also believed to be of upstream origin and not from calcite precipitation. Furthermore, if calcite

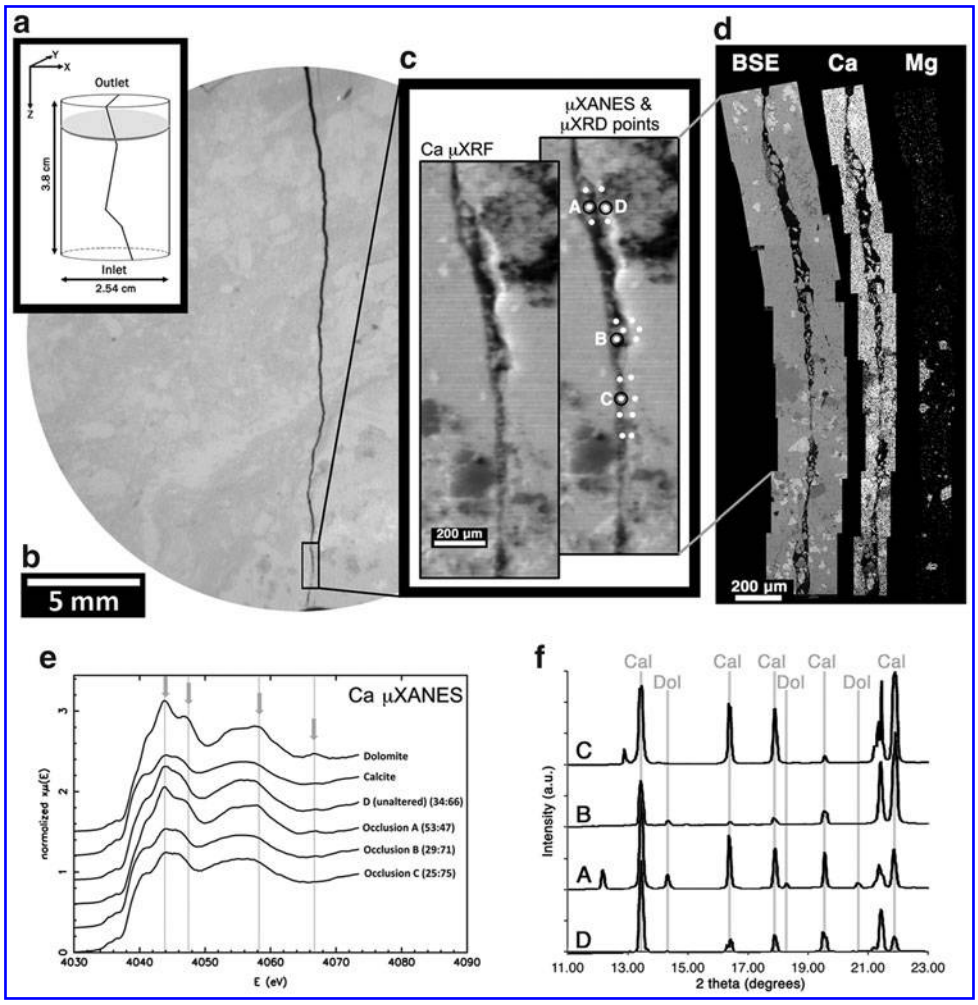

FIG. 4. **(a)** Schematic of fractured core showing core dimensions and location of subsection analyzed throughout Figure 2. **(b)** μCT scan showing evidence of fracture closure. **(c)** μXRFCa elemental map of box highlighted in **(b)** showing locations of μXRD and micro X-ray absorption near edge structure (μXANES) analysis. **(d)** Scanning electron microscope back-scattered electron (BSE) and energy dispersive spectroscopy (EDS) maps for Ca and Mg taken at the same location as **(c)**. **(e)** Ca μXANES spectra for points A–D **(c)**. Calcite and dolomite end-member spectra are also shown along with estimates of dolomite:calcite from linear combination fits. **(f)** μXRD 1D integrated diffraction data for points A–D with corresponding calcite and dolomite peaks indicated.

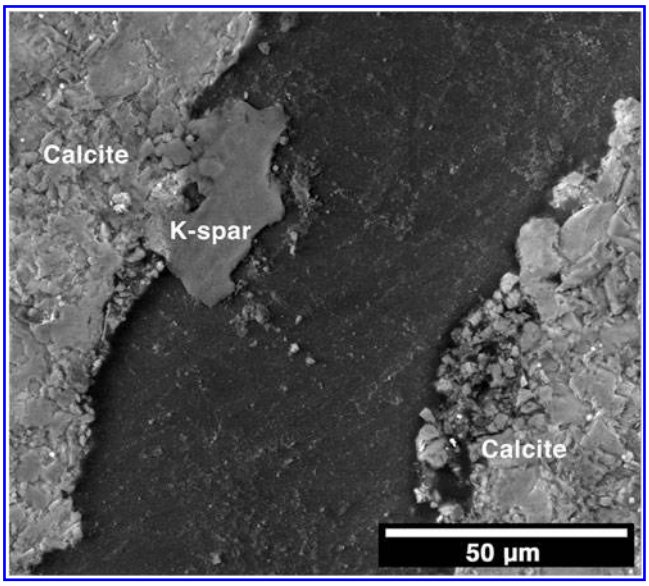

FIG. 5. BSE image showing evidence for dissolution of the calcite matrix surrounding a less reactive mineral grain (K-feldspar). Continuation of this process would have resulted in the release of the K-feldspar grain from the fracture surface.

were to precipitate along the fracture pathway it would be thermodynamically favorable to do so along the calcite-bearing fracture surface (heterogeneous nucleation) rather than within the aqueous phase (homogeneous nucleation) as new particles. Feldspar dissolution and subsequent secondary precipitation of clay minerals is ruled out given the very slow kinetics controlling these reactions and the fact that feldspar minerals were not in abundance (<5% v/v).

Figure 5 provides a visual example of how calcite dissolution can lead to release of less reactive mineral particles. Here calcite dissolution has eroded the rock matrix surrounding a K-feldspar grain. Continued dissolution of the surrounding calcite matrix would have eventually released the grain from the fracture surface. By reasonable conjecture, this is the same way that the dolomite-bearing fragments identified in Fig. 4 were generated.

Discussion

Hypothetically, decreases in fracture permeability due to reactive flows can be attributed to three possible mechanisms: precipitation of secondary minerals in the flow path, occlusion due to particle clogging along the fracture pathway (Noiriel *et al*., 2007; Andreani *et al*., 2008), and dissolution of critical fracture asperities that results in mechanical aperture closure (Polak *et al*., 2003; Yasuhara *et al*., 2006). Although there was a decrease in Ca concentration in the effluent after the flow rate was reduced, calcite precipitation was not identified using any of the imaging methods, so we rule this out as a possible mechanism. Analyses of the particles lodged within the fracture support a scenario where dissolution of calcite led to decohesion and mobilization of less reactive grains that occluded the flow path. Finally, μCT aperture maps suggest that the occluded portion of the fracture produced preferential flow paths along which calcite dissolution removed enough rock mass to eliminate critical asperities and cause mechanical compression of the fracture. Dissolution of critical asperities leading to reduced fracture permeability is consistent with previous studies (Polak *et al.*, 2003). Measurements of mechanical aperture during flow, however, are required to quantify the proportional contribution of these two mechanisms.

These experimental observations of leakage pathway self-sealing shift the focus of efforts to predict permeability evolution from precipitation to coupled geochemical and geomechanical mechanisms. This experiment has shown that calcite dissolution in carbonate rocks may ultimately result in reduced permeability. This is a plausible scenario in formations with compressive stress and in rocks that are mineralogically heterogeneous. This scenario is a counterintuitive result as dissolution is often associated with an increase in porosity, which leads to an increase in permeability. This process would be difficult to predict with existing reactive transport models. Newell and Carey (2012) observed similar fines migration and clogging leading to permeability reductions along a simulated cement-caprock leakage pathway. The observation of dissolution-driven particle migration along a possible CO_2 leakage pathway made by Newell and Carey (2012) supports the findings of our current study, thereby helping to make the case for inclusion of particle transport into future reactive transport simulations assessing CO_2 leakage risk. An excellent example of simulated particle transport and permeability reduction relevant to CO_2 sequestration has been presented by Sbai and Azaroual (2011), although for a porous medium rather than for a fractured caprock, and not due to dissolution-induced particle mobilization. Accounting for potential mechanical closure of the fracture following the approach of the thermal-hydrologic-mechanical-chemical modeling employed for the study of geothermal reservoirs (*e.g.*, Taron and Elsworth, 2009) should also lead to more robust CO_2 leakage risk assessments.

In comparing the findings of this study with those of our previous study, Ellis *et al.* (2011), we find that two very similar experiments performed on nearly identical rock cores resulted in opposite outcomes with respect to fracture permeability evolution. This brings into question the reliability of using only a few bench-scale experiments to validate models that estimate fracture permeability evolution, as each experiment may be unique due to spatial variability in mineralogy and different solution chemistries. Experiments conducted at realistic reservoir conditions on actual caprock samples are needed because they may draw our attention to important processes not captured in current models.

Acknowledgments

This project was supported through funding from the U.S. Department of Energy National Energy Technology Laboratory and U.S. DOE award number DE-FE0000749. B.R.E. acknowledges additional funding support through the ORISE professional internship program and the ASCE Freeman Fellowship. We also acknowledge the use of PRISM Imaging and Analysis Center, which is supported, in part, by the NSF MRSEC program through the Princeton Center for Complex Materials (grant DMR-0819860). BNL and the NSLS operate under U.S. DOE Contract No. DE-AC02-98CH10886. Additional support for Beamline X27A comes from the U.S. DOE under DE-FG02-92ER14244 to the University of Chicago–CARS.

Author Disclosure Statement

No competing financial interests exist.

References

Andreani, M., Gouze, P., Luquot, L., and Jouanna, P. (2008). Changes in seal capacity of fractured claystone caprocks induced by dissolved and gaseous CO_2 seepage. *Geophys. Res. Lett.* 35, L14404; DOI: 10.1029/2008GL034467.

Berkowitz, B., and Balberg, I. (1993). Percolation theory and its application to groundwater hydrology. *Water Resour. Res.* 29, 775.

Celia, M.A., and Nordbotten, J.M. (2009). Practical modeling approaches for geological storage of carbon dioxide. *Ground Water* 47, 627.

Crandell, L.E., Peters, C.A., Um, W., Jones, K.W., and Lindquist, W.B. (2012). Changes in the pore network structure of Hanford sediment after reaction with caustic tank wastes. *J. Contam. Hydrol.* 131, 89.

Duan, Z.H., Sun, R., Zhu, C., and Chou, I.M. (2006). An improved model for the calculation of CO_2 solubility in aqueous solutions containing Na^+, K^+, Ca^{2+}, Mg^{2+}, Cl^-, and SO_4^{2-}. *Mar. Chem.* 98, 131.

Ellis, B.R., Crandell, L.E., and Peters, C.A. (2010). Limitations for brine acidification due to SO_2 co-injection in geologic carbon sequestration. *Int. J. Greenh. Gas Control* 4, 575.

Ellis, B.R., Peters, C.A., Fitts, J.P., Bromhal, G.S., McIntyre, D.L., Warzinski, R.P., and Rosenbaum, E.J. (2011). Deterioration of a fractured carbonate caprock exposed to CO_2-acidified brine flow. *Greenh. Gases Sci. Technol.* 1, 248.

Gherardi, F., Xu, T.F., and Pruess, K. (2007). Numerical modeling of self-limiting and self-enhancing caprock alteration induced by CO_2 storage in a depleted gas reservoir. *Chem. Geol.* 244, 103.

Gouze, P., Noiriel, C., Bruderer, C., Loggia, D., and Leprovost, R. (2003). X-ray tomography characterization of fracture surfaces during dissolution. *Geophys. Res. Lett.* 3, 1267.

Hammersley, A.P., Svensson, S.O., Hanfland, M., Fitch, A.N., and Hausermann, D. (1996). Two-dimensional detector software: From real detector to idealised image or two-theta scan. *High Pressure Res.* 14, 235.

Huerta, N.J., Bryant, S.L., Strazisar, B.R., and Hesse, M. (2011). Dynamic alteration along a fractured cement/cement interface: Implications for long term leakage risk along a well with an annulus defect. *Energy Procedia* 4, 5398.

Kaszuba, J.P., Janecky, D.R., and Snow, M.G. (2005). Experimental evaluation of mixed fluid reactions between supercritical carbon dioxide and NaCl brine: Relevance to the integrity of a geologic carbon repository. *Chem. Geol.* 217, 277.

Ketcham, R.A., and Carlson, W.D. (2001). Acquisition, optimization and interpretation of X-ray computed tomographic imagery: Applications to the geosciences. *Comput. Geosci.* 27, 381.

LeNeveu, D.M. (2008). Cquestra, a risk and performance assessment code for geological sequestration of carbon dioxide. *Energy Convers. Manage.* 49, 32.

Lewicki, J.L., Birkholzer, J., and Tsang, C.F. (2007). Natural and industrial analogues for leakage of CO_2 from storage reservoirs: Identification of features, events, and processes and lessons learned. *Environ. Geol.* 52, 457.

Newell, D.L., and Carey, J.W. (2013). Experimental evaluation of wellbore integrity along the cement-rock boundary. *Environ. Sci. Technol.* 47, 276.

Nogues, J.P., Celia, M.A., and Peters, C.A. (2012). Pore network model development to study dissolution and precipitation of carbonates. In *XIX International Conference on Water Resources CMWR 2012*, edited, Urbana, IL. http://cmwr2012.cee.illinois.edu

Noiriel, C., Made, B., and Gouze, P. (2007). Impact of coating development on the hydraulic and transport properties in argillaceous limestone fracture. *Water Resour. Res.* 43, W09406

Parkhusrt, D.L., and Appelo, C.A.J. (1999). User's guide to phreeqc (version 2)—A computer program for speciation, batch-reaction, one-dimensional transport, and inverse geochemical calculations. *USGS Water Resources Investigations Report*, 99.

Phillips, S.L., Otto, R.J., Ozbek, H., and Tavana, M. (1981). A technical databook for geothermal-energy utilization. *Abstr. Pap. Am. Chem. S.* 181, 36.

Pitzer, K.S. (1973). Thermodynamics of electrolytes .1. Theoretical basis and general equations. *J. Phys. Chem.* 77, 268.

Pokrovsky, O.S., Golubev, S.V., Schott, J., and Castillo, A. (2009). Calcite, dolomite and magnesite dissolution kinetics in aqueous solutions at acid to circumneutral pH, 25 to 150 degrees C and 1 to 55 atm pCO_2: New constraints on CO_2 sequestration in sedimentary basins. *Chem. Geol.* 265, 20.

Polak, A., Elsworth, D., Yasuhara, H., Grader, A.S., and Halleck, P.M. (2003). Permeability reduction of a natural fracture under net dissolution by hydrothermal fluids. *Geophys. Res. Lett.* 3, 2020.

Ravel, B., and Newville, M. (2005). Athena, Artemis, Hephaestus: Data analysis for X-ray absorption spectroscopy using IFEFFIT. *J. Synchrotron Radiat.* 12, 537.

Sbai, M.A., and Azaroual, M. (2011). Numerical modeling of formation damage by two-phase particulate transport processes during CO_2 injection in deep heterogeneous porous media. *Adv. Water Resour.* 34, 62.

Shao, H.B., Ray, J.R., and Jun, Y.S. (2010). Dissolution and precipitation of clay minerals under geologic CO_2 sequestration conditions: CO_2-brine-phlogopite interactions. *Environ. Sci. Technol.* 44, 5999.

Shukla, R., Ranjith, P., Haque, A., and Choi, X. (2010). A review of studies on CO_2 sequestration and caprock integrity. *Fuel* 89, 2651.

Smith, M.M., Sholokhova, Y., Hao, Y., and Carroll, S.A. (2013). Evaporite caprock integrity: An experimental study of reactive mineralogy and pore-scale heterogeneity during brine-CO_2 exposure. *Environ. Sci. Technol.* 47, 262.

Taron, J., and Elsworth, D. (2009). Thermal-hydrologic-mechanical-chemical processes in the evolution of engineered geothermal reservoirs. *Int. J. Rock Mech. Min.* 46, 855.

Viswanathan, H.S., Pawar, R.J., Stauffer, P.H., Kaszuba, J.P., Carey, J.W., Olsen, S.C., Keating, G.N., Kavetski, D., and Guthrie, G.D. (2008). Development of a hybrid process and system model for the assessment of wellbore leakage at a geologic CO_2 sequestration site. *Environ. Sci. Technol.* 42, 7280.

Wigand, M., Kaszuba, J.P., Carey, J.W., and Hollis, W.K. (2009). Geochemical effects of CO_2 sequestration on fractured wellbore cement at the cement/caprock interface. *Chem. Geol.* 265, 122.

Yasuhara, H., Polak, A., Mitani, Y., Grader, A.S., Halleck, P.M., and Elsworth, D. (2006). Evolution of fracture permeability through fluid-rock reaction under hydrothermal conditions. *Earth Planet. Sci. Lett.* 244, 186.

Zhang, C.Y., Dehoff, K., Hess, N., Oostrom, M., Wietsma, T.W., Valocchi, A.J., Fouke, B.W., and Werth, C.J. (2010). Pore-scale study of transverse mixing induced $CaCO_3$ precipitation and permeability reduction in a model subsurface sedimentary system. *Environ. Sci. Technol.* 44, 7833.

Zimmerman, R.W., and Bodvarsson, G.S. (1996). Hydraulic conductivity of rock fractures. *Transport Porous Med.* 23, 1.

This article has been cited by:

1. Hang Deng, Brian R. Ellis, Catherine A. Peters, Jeffrey P. Fitts, Dustin Crandall, Grant S. Bromhal. 2013. Modifications of Carbonate Fracture Hydrodynamic Properties by CO 2 -Acidified Brine Flow. *Energy & Fuels* 130419152646006. [CrossRef]